Geophysical Research Letters

RESEARCH LETTER
10.1029/2022GL099731

Solid Earth Uplift Due To Contemporary Ice Melt Above Low-Viscosity Regions of the Upper Mantle

Maaike F. M. Weerdesteijn[1], Clinton P. Conrad[1], and John B. Naliboff[2]

[1]Centre for Earth Evolution and Dynamics, University of Oslo, Oslo, Norway, [2]Department of Earth and Environmental Science, New Mexico Institute of Mining and Technology, Socorro, NM, USA

Key Points:

- Contemporary ice melt above low-viscosity mantle produces uplift on decadal timescales, but viscosity heterogeneity affects uplift rates
- Our viscoelastic deformation models with varying viscosity show that a low-viscosity region's horizontal extent greatly affects uplift rates
- The viscous response to recent ice melting, usually not considered, may be a dominant contributor to uplift above low-viscosity regions

Supporting Information:

Supporting Information may be found in the online version of this article.

Correspondence to:

M. F. M. Weerdesteijn,
m.f.m.weerdesteijn@geo.uio.no

Citation:

Weerdesteijn, M. F. M., Conrad, C. P., & Naliboff, J. B. (2022). Solid earth uplift due to contemporary ice melt above low-viscosity regions of the upper mantle. *Geophysical Research Letters*, *49*, e2022GL099731. https://doi.org/10.1029/2022GL099731

Received 24 MAY 2022
Accepted 1 SEP 2022

Author Contributions:

Conceptualization: Maaike F. M. Weerdesteijn, Clinton P. Conrad
Formal analysis: Maaike F. M. Weerdesteijn
Funding acquisition: Clinton P. Conrad
Methodology: Maaike F. M. Weerdesteijn
Software: Maaike F. M. Weerdesteijn, John B. Naliboff
Supervision: Clinton P. Conrad
Visualization: Maaike F. M. Weerdesteijn
Writing – original draft: Maaike F. M. Weerdesteijn
Writing – review & editing: Clinton P. Conrad, John B. Naliboff

Abstract Glacial isostatic adjustment explains topographic change in formerly and currently glaciated regions, but the role of small (~100s km) regions of unusually low-viscosity mantle is poorly understood. We developed viscoelastic models with low-viscosity regions in the upper mantle, and measured the effect of these regions on solid earth uplift resulting from contemporary surface ice melt. We found viscous uplift occurring on decadal timescales above the low-viscosity region, at rates comparable to or larger than those from elastic uplift or the viscous response to ice age melting. We find that uplift rates are sensitive to the location, dimensions, and viscosity of the low-viscosity region, and that the largest uncertainty in uplift rates likely comes from the low-viscosity region's horizontal extent. Rapid viscous ground uplift can impact ice dynamics if the low-viscosity region is located close to an ice sheet margin, as for Antarctica and Greenland.

Plain Language Summary Ice melting in Antarctica and Greenland causes ground motion as Earth's interior rocks deform in response to ice mass changes at the surface. The timescale on which the deformation takes place is dependent on the capacity of the interior rocks to deform, controlled by viscosity. It is commonly thought that high viscosity in the mantle causes deformation to take place on timescales of thousands of years. However, low-viscosity regions speed up the deformation considerably, taking decades instead. We developed numerical models that can handle large spatial variations in viscosity. We found that contemporary ice melt above a low-viscosity region can cause upward deformation at rates faster than from the past (ice age) melting, and large enough to be an important consideration for understanding future ice dynamics in potential rapid melting scenarios.

1. Introduction

Glacial isostatic adjustment (GIA) is the ongoing response of the solid earth and the geoid to changes in ice and ocean loading, and produces solid earth ground motion that can be measured using GNSS (Global Navigation Satellite Systems). Near areas of past or current ice cover change, it is commonly thought GIA displacements result from a combination of (a) a viscous response to historic ice load changes (i.e., ice age melting), and (b) an elastic response to contemporary ice load changes. Typically, the viscous response occurs over several thousand years, but recent studies have shown regions undergoing rapid viscous uplift on decadal or centennial timescales in response to contemporary ice melt in West Antarctica (Barletta et al., 2018; Nield et al., 2014) and southeast Greenland (Khan et al., 2016). Rapid uplift in these regions is commonly linked to low-viscosities in the upper mantle that accelerate the viscous response to recent melting. In this case, contemporary ice melt generates not only an instantaneous elastic response, but also a viscous response on short timescales. This rapid viscous response is mixed with the other deformation components of GIA (elastic and long-term viscous) that are measured using GNSS, which makes it difficult to distinguish between solid earth deformation due to historical and contemporary ice load changes (Whitehouse, 2018).

There are indications that low-viscosity regions of the upper mantle are present beneath both Antarctica and Greenland. Here, we define low-viscosity regions as regions where the viscosity is considerably lower than surrounding mantle material, with a value that can result in deformation on decadal or centennial timescales (e.g., $5 \cdot 10^{19}$ Pa s or lower), as opposed to thousands of years. Seismic studies in Antarctica show slower velocity anomalies in West compared to East Antarctica (Heeszel et al., 2016; Lloyd et al., 2020), consistent with a colder cratonic region in East Antarctica, and a warmer tectonically active region in West Antarctica, possibly with a mantle plume (Bredow et al., 2021). Lateral variations in mantle temperature, derived from seismic velocity anomalies, suggest lateral variations in mantle rheology (Ivins & Sammis, 1995; van der Wal et al., 2013). Upper

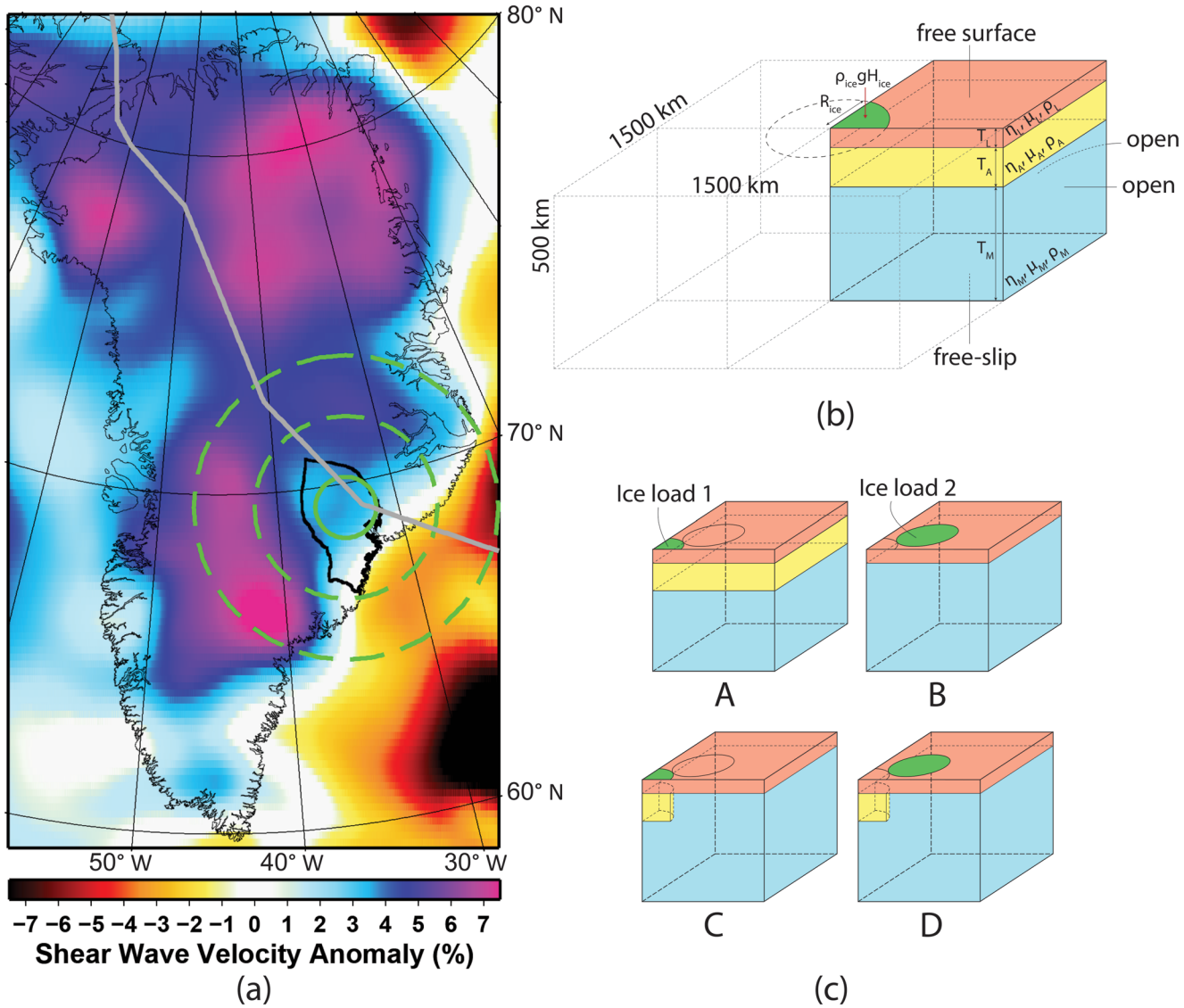

Figure 1. (a) Seismic velocity anomalies at 150 km depth for Greenland (Celli et al., 2021). The gray line represents the potential plume track, drawn following Martos et al. (2018), the black bordered area is the drainage basin where the Kangerlussuaq glacier is located, and the inner green circle is the size of the modeled ice load and low-viscosity region (100 km radius), plus dashed green circles with radii of 300 and 500 km. (b) A quarter of the box model geometry (not to scale) with upper mantle (blue), low-viscosity asthenosphere (yellow), lithosphere (red), and active ice load (green), boundary conditions, layer properties, and boundary traction from ice loading. (c) Cases A and B showcase the 1D approach and cases C and D showcase the 3D approach for the two ice loads.

mantle viscosities constrained by GNSS uplift and ice mass change show large variations across the Antarctic Peninsula and the Amundsen Sea Embayment, ranging from $<3 \cdot 10^{18}$ Pa s to $3 \cdot 10^{20}$ Pa s (Barletta et al., 2018; Nield et al., 2014; Wolstencroft et al., 2015).

The Kangerlussuaq glacier in southeast Greenland, one of Greenland's three largest ice mass losing glaciers (Brough et al., 2019), sits above a proposed upper mantle low-viscosity feature that is likely as a consequence of Greenland having passed over the Iceland plume more than 40 Myr ago (Steinberger et al., 2019). Proposed hot spot tracks align with magnetic, temperature, gravity, and seismic data (Celli et al., 2021; Martos et al., 2018; Mordret, 2018; Rogozhina et al., 2016; Steffen et al., 2018) and suggest a weakened lithosphere and upper mantle (Figure 1a). Khan et al. (2016) suggested that GNSS uplift rates are consistent with a low-viscosity upper mantle of $1 \cdot 10^{19}$ Pa s beneath southeast Greenland, but their modeled uplift rates are based on a summation of deformation solutions from discretized ice loads above laterally homogeneous (1D) earth models. Milne et al. (2018) explored the influence of laterally heterogeneous (3D) earth structure on GIA in Greenland, but to this day no reconciliation is reached yet between modeled and observed uplift rates.

From seismic tomography models (Celli et al., 2021; Lloyd et al., 2020), we know there is a limited horizontal and vertical extent to potential low-viscosity regions beneath the lithosphere for Antarctica and Greenland (Figure 1a). As yet, no study has systematically examined the sensitivity of uplift patterns to the dimensions, location, and viscosity of a low-viscosity region deforming as a result of contemporary ice melting, nor has any study characterized which parameter(s) contribute(s) dominantly to the uplift signal. The purpose of this study is to provide this systematic understanding in order to evaluate whether 3D modeling is important. To investigate this sensitivity, we compute viscoelastic earth deformation caused by contemporary ice melt above both a homogeneous earth (1D) and a heterogeneous earth (3D). By varying the dimensions, location, and viscosity of a low-viscosity region, we determine their effect on patterns and rates of uplift.

2. Modeling Deformation Near a Low-Viscosity Region: 1D Versus 3D Approach

We compare solid earth deformation due to contemporary ice melt for two modeling approaches, a 1D and 3D approach. The 1D approach consists of a summation of deformation solutions from discretized ice loads above layered viscosity structures. The 3D approach incorporates a low-viscosity (LV) region. In this study, we use an open-source, finite-element based, viscoelastic earth deformation model in ASPECT v2.3.0 (Advanced Solver for Problems in Earth's ConvecTion) (Bangerth et al., 2021a, 2021b). For the GIA simulations, ASPECT solves the 3-D incompressible conservation equations assuming an infinite Prandtl number, the Boussinesq approximation, and isothermal flow, and assuming linear viscoelasticity (Moresi et al., 2003; Sandiford et al., 2021) (see Texts S1 to S3 in Supporting Information S1 for the model's mathematical description).

Model properties are shown in Figure 1b and Table S1 in Supporting Information S1 (Dziewonski & Anderson, 1981). We use a box geometry with a horizontal dimension of 1,500 km in both directions and vertical dimension of 500 km, introducing a <0.05% error compared to a very wide (3,000 km) box, and a 0.5% error compared to a box of earth mantle depth (~3,000 km). We use a linear Maxwell viscoelastic rheology. The top boundary is a free surface (Rose et al., 2017), allowing for vertical and lateral mesh deformation, and the bottom boundary is free-slip, allowing for tangential material flow only. The lateral boundaries are open, allowing for material in- and outflow, by applying boundary traction based on the lithostatic pressure profile. The ice loading consists of two cylindrical loads with a 100 km radius (approximate drainage basin size, Figure 1a), 931 kg/m^3 ice density, and constant height in space. The ice height linearly decreases from 100 to 0 m over 100 years, that is, 1 m/yr ice melt, which is the order of magnitude for contemporary ice melt in Antarctica and Greenland (Helm et al., 2014; The IMBIE Team, 2019). Ice load 1 is located in the center of the domain, and ice load 2 is offset by $x = y = \sqrt{2{R_{ice}}^2}$, such that the ice loads touch, but do not overlap (Figure 1c).

In the 1D approach, solid earth deformations are summed for a solution in which ice load 1 is above an LV layer (Figure 1c.A), also referred to as LV asthenosphere, and a solution in which ice load 2 is above an earth structure without an LV layer (Figure 1c.B). In the 3D approach, the same ice loads are placed on an earth model with an LV region (different from an LV layer as it has lateral boundaries), located in the upper mantle underneath ice load 1. In the 3D approach, the simulation is also split into two cases, one for each ice load (Figure 1c.C and 1c.D), to be able to distinguish between the deformations resulting from each ice load to compare to the solutions of the 1D approach (Figure 2). Simulating the two ice loads separately or together results in essentially the same results, as expected for a linear system. The earth model for case A is given in Table S1 in Supporting Information S1. In case B, without an LV asthenosphere, the mantle extends to the bottom of the lithosphere. In cases C and D the LV region has the same material properties as the LV asthenosphere, and a radius equal to the ice load radius of 100 km (consistent with the potential low-viscosity feature size, Figure 1a). The asthenosphere has a viscosity of $1 \cdot 10^{19}$ Pa s (background mantle viscosity is $5 \cdot 10^{20}$ Pa s), which is in the plausible range of LV features in West Antarctica and southeast Greenland (Khan et al., 2016; Nield et al., 2014). Using adaptive mesh refinement (i.e., the mesh automatically adjusts itself with time), we have a resolution ranging between 3.625 and 50 km, with higher resolution within volumes of higher strain rate. The numerical time step size is 2.5 years.

The vertical surface deformation due to ice load 1 above the LV asthenosphere (Figure 2, case A) is ~2.5 times larger than for the ice load above the LV region (Figure 2, case C). This is because the ice load is sensitive not only to the viscosity structure directly underneath it, but also to the viscosities surrounding the load. Furthermore, case A shows subsidence in the periphery, about 300 km away from the ice load center. These areas of subsidence (or bulges in case of ice load increase) are a result of the LV layer that allows for channel flow (Cathles, 1975).

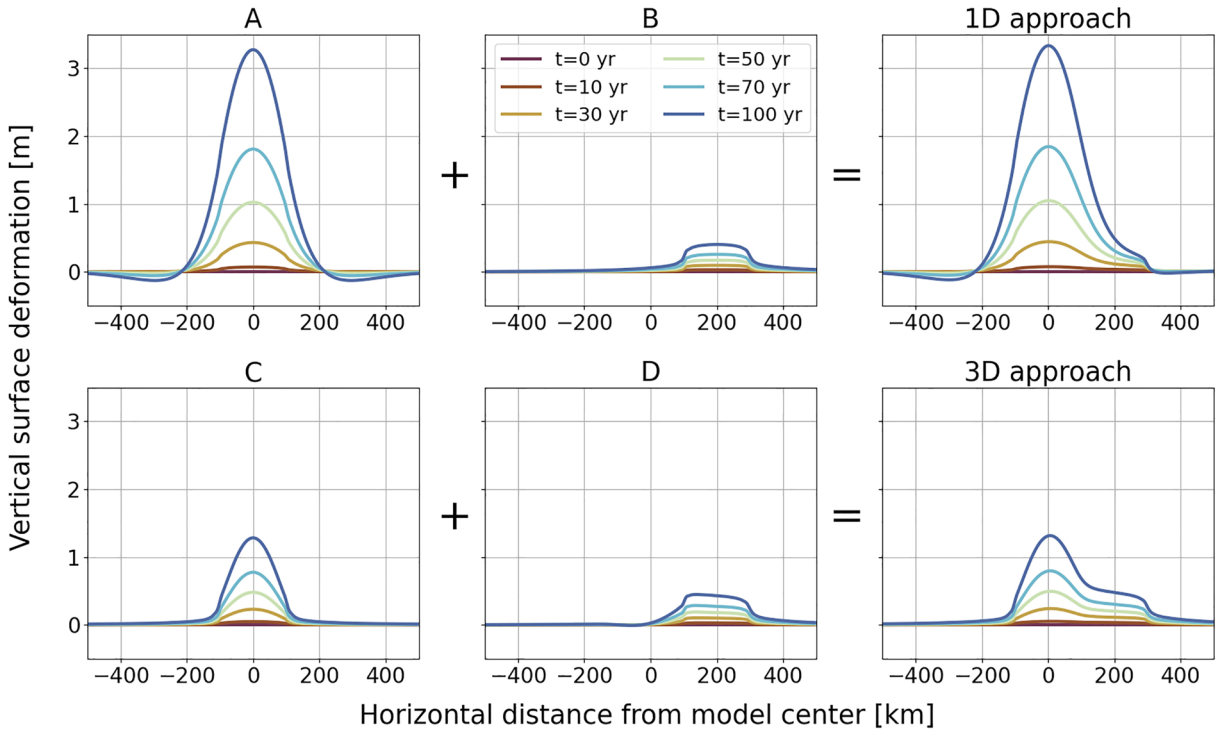

Figure 2. Vertical surface deformation as a function of the horizontal distance from the model center at different time intervals (colors) for case A, case B, the total solution from the 1D approach (upper right), case C, case D, and the total solution from the 3D approach (lower right). See Figure 1c for depictions of the different cases.

The areas of subsidence are not present in the 3D solution as there is no LV channel present (Figure 2, case C). The deformation due to ice load 2 in the 3D approach is skewed toward the LV region, and is slightly larger than for the 1D approach (Figure 2, case D). The total deformation for the 1D and 3D approaches is very different in magnitude and spatial pattern (Figure 2, right column). This emphasizes the importance of using 3D earth models for solid earth deformation studies from contemporary ice melt in the presence of an LV region, and not a summation of discretized ice loads above different 1D earth models (Hartmann et al., 2020; Khan et al., 2016).

3. Sensitivity of Deformation to Low-Viscosity Region Characteristics

Now that we have established that in the presence of an LV region the 3D approach provides a more accurate, and different, solution than the 1D approach, we use our 3D modeling tool to look into how the LV region affects solid earth deformation, by varying parameters that describe the LV region. These parameters are the LV region thickness, radius, depth, and viscosity, the distance between the LV region and the ice load (measured between the centers), and the ice load radius. The maximum vertical surface deformation (Figure 3) and rate (Figure 4) at 100 years give insight into how these parameters affect solid earth deformation. We chose parameter ranges to span the range of influence of each parameter.

The reference earth model and ice load are as in case C in the previous section. For the distance between the LV region and the ice load we use the full box geometry. For the other parameters tested (Figures 3 and 4), we take advantage of model symmetry and use a quarter of the box model geometry (as shown in Figure 1b), but with free-slip conditions on the left and front lateral boundaries. We limit the model horizontal dimension to 500 km (reduced from 1,500 km used for Figure 2), introducing only a <0.5% error compared to a very wide (~3,000 km) box, and resulting in a ~3 times faster computation for case C (18 vs. 53 min on 512 CPU).

For a purely elastic case (viscosities in all layers are set to $1 \cdot 10^{40}$ Pa s) the maximum deformation rate is 1.4 mm/yr. The elastic contribution to the deformation rate at 100 years is 5% for case A, 53% for case B, 15% for case C, and 48% for case D. Thus, the viscous contribution to the deformation rate is of comparable size (for cases B and D) or larger than (for cases A and C) the elastic contribution, in the presence of a low-viscosity feature (Figure 4).

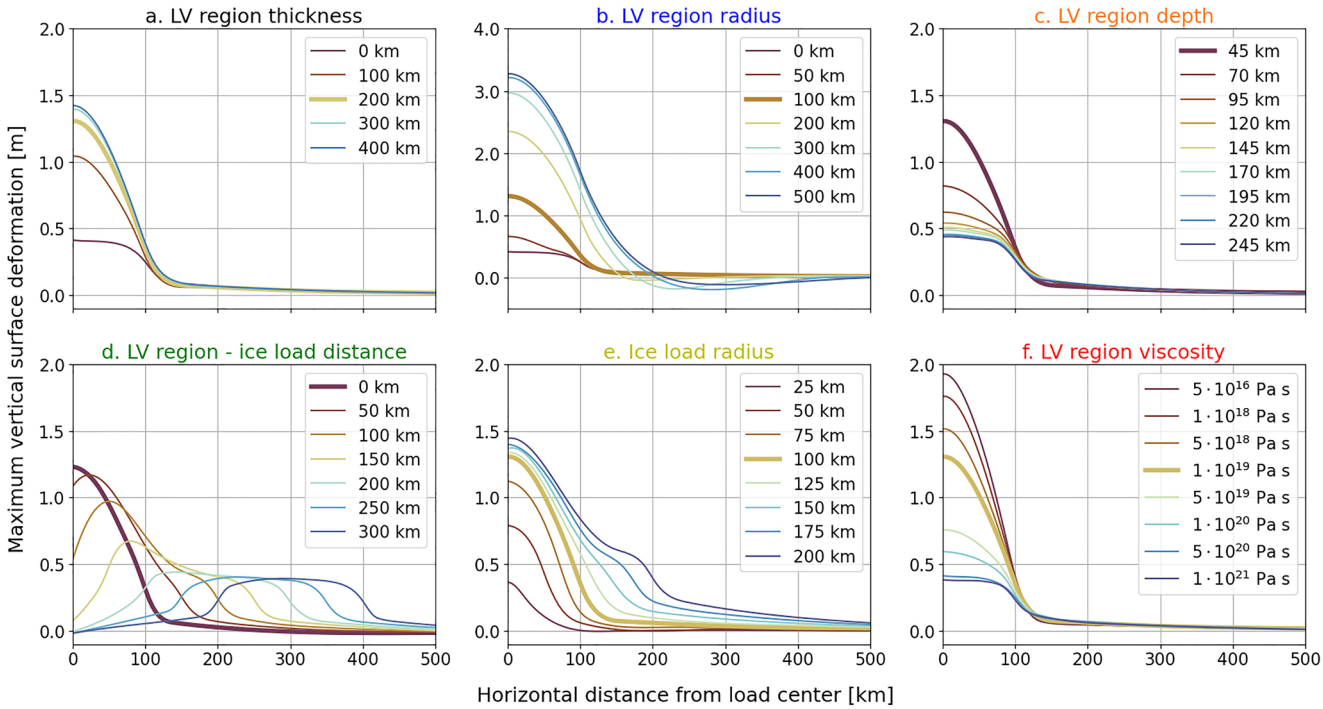

Figure 3. Maximum vertical surface deformation (at $t = 100$ years) as function of horizontal distance from the ice load center for the (a) LV region thickness, (b) LV region radius, (c) LV region depth, (d) distance between the LV region and ice load center, (e) ice load radius, and (f) LV region viscosity. Each colored line represents a variation of the given parameter, and the thick line refers to the parameter value used in the reference case. Note that for the LV region radius (b) the *y* axis range is doubled.

3.1. Low-Viscosity Region Thickness

We vary the LV region thickness from 0 km (no LV region) to 400 km. The maximum vertical surface deformation increases with increasing LV region thickness (Figure 3a), by a factor of ∼3. The maximum rate ranges from 2.6 to 10.2 mm/yr (Figure 4a), a factor ∼4 difference. The deformation saturates for thicknesses greater than 200 km, for which the rate already reaches 9.1 mm/yr.

3.2. Low-Viscosity Region Radius

We vary the LV region radius from 0 km (no LV region) to 500 km (approximating an LV asthenosphere). The maximum vertical surface deformation increases with increasing LV region radius (Figure 3b). Standing out is the subsidence in the periphery of the ice load (also seen in Figure 2, case A), which appears when the LV region radius is larger than the ice load radius (i.e., >100 km). Of all six parameters, the LV region radius produces the largest range in deformation rates, from 2.6 to 26.6 mm/yr (Figure 4b), a factor ∼10 difference.

3.3. Low-Viscosity Region Depth

We vary the LV region depth (defined at the upper surface of the LV region) from 45 km (top surface immediately below the elastic lithosphere) to 245 km. The maximum vertical surface deformation decreases with an increase in LV region depth (Figure 3c), by a factor of ∼3. At a depth of 245 km, the presence of the LV region is barely apparent and approximates the solution for no LV region (as case B). The LV region thus is most important at shallower depths, with a drop in deformation rate from 9.1 to 3.3 mm/yr for an LV region depth from 45 to 145 km, nearly a factor 3 difference (Figure 4c).

3.4. Low-Viscosity Region and Ice Load Distance

We vary the distance between the LV region and ice load from 0 km (overlapping) to 300 km (100 km between the boundaries of the two). The maximum vertical surface deformation decreases if the LV region is farther away

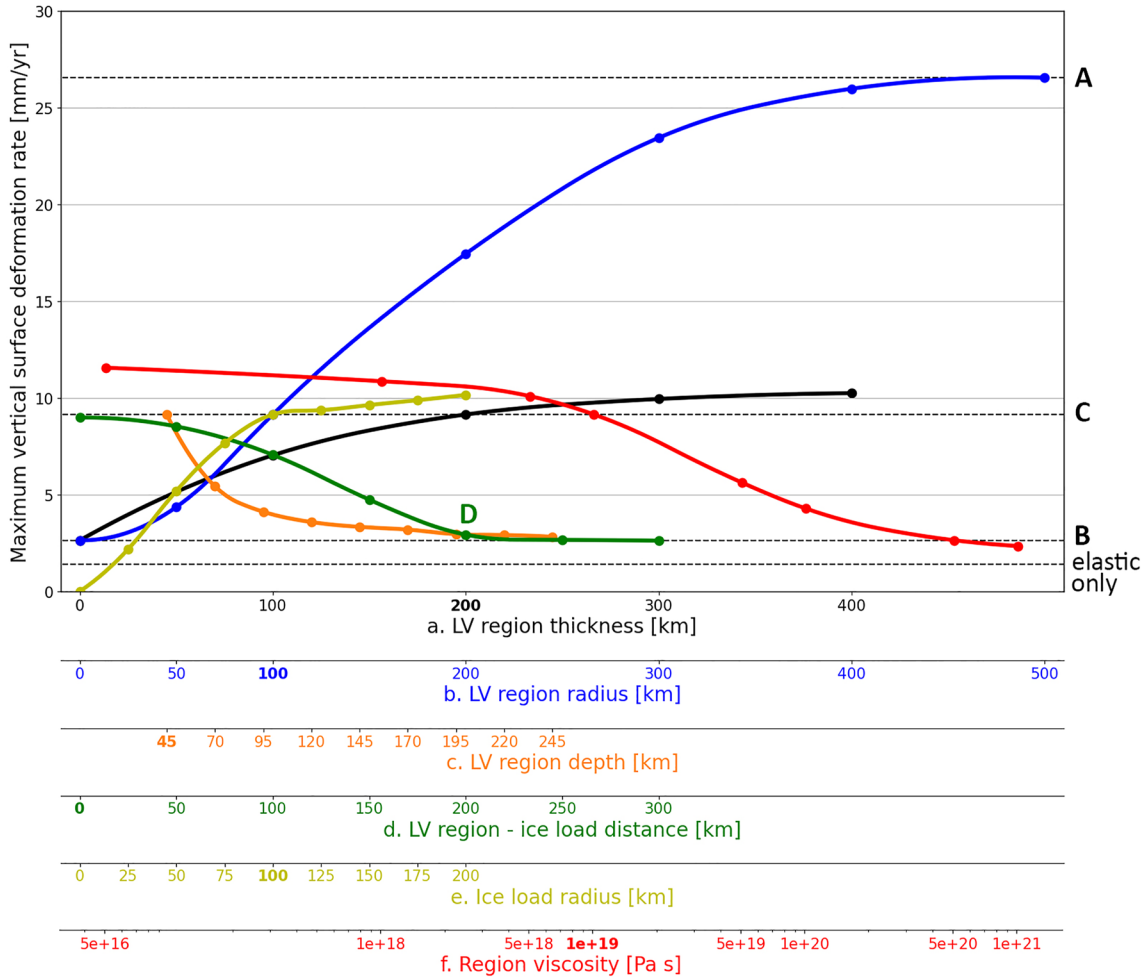

Figure 4. Maximum vertical surface deformation rate (at $t = 100$ years) as function of the (black) LV region thickness, (blue) LV region radius, (orange) LV region depth, (green) distance between the LV region and ice load center, (yellow) ice load radius, and (red) LV region viscosity (colors refer to lines and corresponding x axes). The colored dots indicate model runs and the lines are second order spline interpolated values. The four horizontal dashed lines correspond to cases A, B, C, and purely elastic, and the green dot labeled D corresponds to case D (See Figure 1c for the cases). For each given parameter, the bold values on the x axes represent the parameter value used in the reference case.

from the ice load (Figure 3d). The location of maximum deformation moves with the location of the ice load and the deformation profile becomes increasingly asymmetric. For distances larger than 200 km, the deformation beneath the ice load is no longer sensitive to the LV region. In this case, deformation profiles become symmetric again, and uplift rates of 2.6 mm/yr approximate rates for earth models without an LV region (Figure 4d).

3.5. Ice Load Radius

We vary the ice load radius from 25 to 200 km (twice as large as the LV region radius). The maximum vertical surface deformation increases with the ice load radius, by a factor of ∼4 (Figure 3e). There is little change in the maximum deformation and rate for ice load radii larger than the LV region radius of 100 km (Figures 3e and 4e). For ice load radii larger than 100 km, however, we predict large deformations for distances greater than the LV region radius. The deformation of this second bulge saturates around 0.5 m, which is comparable to the uplift expected without an LV region (case B), as this outer part of the ice load cannot sense the LV region.

3.6. Low-Viscosity Region Viscosity

We vary the LV region viscosity from $5 \cdot 10^{16}$ Pa s to $1 \cdot 10^{21}$ Pa s (a higher viscosity than the surrounding mantle). The maximum vertical surface deformation decreases with an increase in LV region viscosity, by a factor

~5 (Figure 3f). The maximum rate ranges from 11.6 to 2.3 mm/yr (Figure 4f), but changes little for viscosities lower than $1 \cdot 10^{19}$ Pa s (from 9.1 to 11.6 mm/yr). On the other hand, increasing the viscosity by one order of magnitude (from $1 \cdot 10^{19}$ to $1 \cdot 10^{20}$ Pa s) slows the uplift rate by more than a factor of 2 (from 9.1 to 4.3 mm/yr).

4. Discussion

4.1. Factors Affecting Uplift From Contemporary Ice Melt

Uncertainty in the location, viscosity, and even more so dimensions, of an LV region translates directly into uncertainty in the uplift and uplift rates resulting from contemporary ice melt. The largest uncertainty in uplift rates comes from the horizontal extent of the LV region (Figures 3b and 4b), where we see that expanding the LV region size can nearly triple uplift rates. Furthermore, we identify ranges of parameter values for which small variations lead to large differences in uplift rates (Figure 4). These parameter ranges are the LV region thickness up to 200 km, LV region depth up to 145 km, ice load radius up to 100 km (i.e., up to the LV region radius), LV region and ice load distance up to 200 km, and LV region viscosities up to 50 times smaller than the surrounding mantle. Moreover, the LV region radius, distance between the LV region and ice load, and ice load radius greatly impact the spatial pattern of deformation (Figure 3).

Although we employ a linear Maxwell viscoelastic rheology in this study, other more complex rheologies are likely for the mantle. Ivins et al. (2021) described three different flow laws to derive lateral viscosity variations from a seismic model. These flow laws either assume diffusion creep (used in this study), dislocation creep, or a combination of both (i.e., composite flow law). The choice of flow law can locally result in subsurface viscosities that vary by several orders of magnitude depending on the flow law. Large uncertainties may also arise from unknown variability in grain size, water content, and composition (van der Wal et al., 2015). Recent studies explore time- and stress-dependent viscosity (i.e., transient rheology) (Kang et al., 2022) in Antarctica (Blank et al., 2021; Lau et al., 2021) and Greenland (Adhikari et al., 2021). For example, several studies focused on similar locations have resulted in different estimates for mantle viscosity and lithosphere thickness based on historical sea level data and present-day deformation. Lau et al. (2021) argued that these different estimates result from different timescales of deformation and that transient, frequency-dependent, rheology may play an important role on GIA timescales. Kang et al. (2022) showed that stress-dependent rheology causes temporal variations in upper mantle viscosity due to stress variations during the last deglaciation (ended 8,000 years ago), and that the effects can be rather localized (i.e., affecting load-proximal stresses but not far field stresses). Such rheological complexity may also contribute to, or even generate, confined regions with effectively low viscosity, of the sort that we have modeled here. Regardless, the impact of rheological complexity needs more investigation and could help to reconcile models and observations of uplift (Adhikari et al., 2021; Blank et al., 2021; Lau et al., 2021).

4.2. Importance of Contemporary Ice Melt for Greenland Uplift

Bevis et al. (2012) found that in most of coastal Greenland the elastic response to contemporary ice mass change matches the historic viscous response or dominates the uplift signal. However, we show that the viscous response from contemporary ice melt can also significantly contribute to the total uplift, and is a component that is not commonly considered. Simpson et al. (2011) did consider the viscous response from contemporary ice melt, but applied a radially symmetric earth viscosity structure. For areas of rapid ice mass loss near low-viscosity regions of the upper mantle, uplift may be dominated by recent or contemporary ice melt instead of by historic ice melt from the last deglaciation. Furthermore, we show that the GIA signal from contemporary ice change may not grow linearly over short timescales in the presence of an LV region (Figure 2, compare deformation at 50 vs. 100 years). This can complicate (a) studies in which GNSS uplift rates are corrected for GIA from historic ice load changes and the remaining (assumed elastic) deformation is used to constrain contemporary ice discharge, an approach that Hansen et al. (2021) used to constrain mass loss from Greenland's three largest outlet glaciers, and (b) studies in which an elastic correction for contemporary ice change is applied to GNSS uplift rates to infer the GIA signal from past ice change, because the viscous response from contemporary ice change is not considered.

4.3. 1D Versus 3D Modeling for Greenland

The 1D approach adopted by, for example, Khan et al. (2016) to estimate ice history and earth rheology in Greenland may be valid for some regions of Greenland, but perhaps not for southeast Greenland, which is likely

characterized by a confined LV region in the upper mantle (Figure 1a). By applying a layered viscosity structure per drainage basin, Khan et al. (2016) effectively expanded the LV feature in southeast Greenland infinitely (as a full LV asthenospheric layer) for the ice loss in that region. We show that using a wide LV region highly overestimates uplift rate, by up to 3 times, if the actual LV region is confined. Figure 1a shows that an LV region of 300 km radius already overlaps with larger positive velocity anomalies in the upper mantle, indicating higher viscosity. Our modeled uplift rates show that there is a significant reduction in rates for LV regions with a radius smaller than 300 km compared to an LV asthenospheric layer (Figure 4b). This means that to reconcile models and observations of uplift using a 3D approach instead of a 1D approach (i.e., to achieve larger modeled uplift rates with a 3D approach), the ice melt must be larger/faster and/or the LV region must be even shallower (Figure 4c) or have an even lower viscosity (Figure 4f) than considered here. Alternatively, more complex creep mechanisms need to be considered (Section 4.1). Furthermore, the 1D approach generates subsidence across a wide horizontal extent of the LV region, due to channel flow.

The 1D approach, regardless of the presence of an LV layer, may be valid for long-wavelength loading in the far field (Hartmann et al., 2020), but it is not a valid approach near an LV region, because it does not account for stresses that are transmitted through rheological boundaries. Furthermore, even if the LV region is very wide (e.g., as wide as the drainage basin), deformation in neighboring drainage basins (without an LV layer) may also be affected (Figures 3d and 4d) because the influence of a nearby LV region cannot be captured in the 1D approach. A 1D approach may be valid in regions with a broad LV region, as Marsman et al. (2021) found for Alaska, where lateral viscosity variations ($1.6 \cdot 10^{19}$ to $5.0 \cdot 10^{19}$ Pa s in the shallow upper mantle) across a broad region (1,425 by 2,325 km) did not improve the fit to observations compared to a 1D model. However, southeast Greenland is likely characterized by a confined LV region (Figure 1a) that is small enough to significantly reduce uplift rates compared to a 1D case (LV layer). For Antarctica, there are large viscosity variations between East and West Antarctica, and even within West Antarctica and the Antarctic Peninsula seismic velocity anomalies vary greatly in the upper mantle (Lloyd et al., 2020). A 1D approach may be accurate for selected regions where the viscosity does not vary much laterally over a wide region, but not near rheological boundaries.

4.4. Ice Sheet and Glacier Dynamics

Rapid uplift from contemporary ice melt may also impact ice sheet and glacier dynamics. When ice melts, the surface elevation decreases and the ice is subjected to warmer temperatures and larger melt rates, leading to further ice melt, and potential ice sheet destabilization (Levermann et al., 2013). However, GIA counteracts this feedback by increasing the surface elevation when ice melts (Zeitz et al., 2022), and fast uplift above LV regions can amplify this feedback. For marine terminating glaciers, GIA can stabilize the grounding line. Ice melt far from the grounding line results in local sea level rise and potential grounding line retreat, while ice melt close to the grounding line (i.e., close enough to trigger isostatic effects at the grounding line) causes solid earth uplift and local sea level fall, leading to grounding line advance if the viscoelastic response is large/fast enough to counteract the ice thinning (Whitehouse, 2018; Whitehouse et al., 2019). Thus, near LV regions with rapid solid earth uplift, this feedback may limit future ice loss (Gomez et al., 2015, 2018; Kachuck et al., 2020; Konrad et al., 2015; Pollard et al., 2017). The feedback of local sea level change on grounding line position is more evident in Antarctica than Greenland, as most marine terminating glaciers in Greenland do not have large floating ice sections (Khan et al., 2020). However, grounding line positions, and thus stability, of these glaciers are affected by solid earth uplift due to ice thinning. West Antarctica is characterized by low upper mantle viscosities (although absolute mantle viscosity is still poorly constrained and could benefit from an inversion using a variety of geophysical data (Ramirez et al., 2022)), and large ice mass loss (The IMBIE Team, 2018); a combination that may help to stabilize the ice sheet.

5. Conclusion

Our viscoelastic deformation models show that contemporary ice melt generates not only an elastic response of the solid earth but also a viscous response. If the melting occurs near a low-viscosity region of the upper mantle, then this viscous response can be larger than the elastic response (Figure 4f). With such a large viscous contribution, uplift in areas of large ice melt can be controlled by recent or contemporary ice melt instead of by historic ice melt from the last deglaciation. From a sensitivity analysis of the location, dimensions, and viscosity of an LV region, we find that the largest uncertainty in uplift rates from contemporary ice melt comes from the

horizontal extent of the LV region. We find that uplift from contemporary ice melt can be as much as 10 times larger for a very wide (essentially infinite) LV region than it is without an LV region, and a confined LV region produces intermediate rates. Our modeled uplift rates show that there is a significant reduction in rates for LV regions with a radius smaller than 300 km compared to an LV asthenospheric layer (Figure 4b). Thus, 3D modeling is important near areas of reduced viscosity in the upper mantle. As the LV region amplifies GIA uplift from contemporary ice melt, it is important to constrain the location, dimensions, and viscosity of an LV region in order to distinguish between uplift generated by past and contemporary ice melt. Rapid viscous ground uplift can impact ice dynamics if the low-viscosity region is located close to an ice sheet margin, as for Antarctica and Greenland.

Data Availability Statement

The open-source code ASPECT (v2.3.0) (Bangerth et al., 2021b) is available for download on GitHub (https://github.com/geodynamics/aspect/releases/tag/v2.3.0) or Zenodo (https://doi.org/10.5281/zenodo.5131909), along with an example parameter file for the reference case (https://doi.org/10.5281/zenodo.6861410). In Figures 2 and 3 the scientific cyclic color map romaO is used (Crameri, 2018).

Acknowledgments
The authors thank an anonymous reviewer and Pippa Whitehouse for their reviews, which helped us to improve the manuscript, and Rebekka Steffen for her feedback on the 1D versus 3D modeling. This work was supported by the Norwegian Research Council projects 223272 (Centre of Excellence) and 288449 (MAGPIE Project). Computations were made possible by the Norwegian Research Infrastructure Services (NRIS) via allocations NN9283K/NS9029K. We thank the Computational Infrastructure for Geodynamics (geodynamics.org), which is funded by the National Science Foundation under award nos. EAR-0949446 and EAR-1550901, for supporting the development of ASPECT.

References

Adhikari, S., Milne, G. A., Caron, L., Khan, S. A., Kjeldsen, K. K., Nilsson, J., et al. (2021). Decadal to centennial timescale mantle viscosity inferred from modern crustal uplift rates in Greenland. *Geophysical Research Letters*, *48*(19). https://doi.org/10.1029/2021GL094040

Bangerth, W., Dannberg, J., Fraters, M., Gassmoeller, R., Glerum, A., Heister, T., & Naliboff, J. (2021a). ASPECT: Advanced solver for problems in Earth's ConvecTion, User manual. https://doi.org/10.6084/m9.figshare.4865333

Bangerth, W., Dannberg, J., Fraters, M., Gassmoeller, R., Glerum, A., Heister, T., & Naliboff, J. (2021b). ASPECT v2.3.0. *Zenodo*. https://doi.org/10.5281/zenodo.5131909

Barletta, V., Bevis, M., Smith, B., Wilson, T., Brown, A., Bordoni, A., et al. (2018). Observed rapid bedrock uplift in Amundsen Sea embayment promotes ice-sheet stability. *Science*, *360*(6395), 1335–1339. https://doi.org/10.1126/science.aao1447

Bevis, M., Wahr, J., Khan, S. A., Madsen, F. B., Brown, A., Willis, M., et al. (2012). Bedrock displacements in Greenland manifest ice mass variations, climate cycles and climate change. *Proceedings of the National Academy of Sciences*, *109*(30), 11944–11948. https://doi.org/10.1073/pnas.1204664109

Blank, B., Barletta, V., Hu, H., Pappa, F., & van der Wal, W. (2021). Effect of lateral and stress-dependent viscosity variations on GIA induced uplift rates in the Amundsen Sea embayment. *Geochemistry, Geophysics, Geosystems*, *22*(9), e2021GC009807. https://doi.org/10.1029/2021GC009807

Bredow, E., Steinberger, B., Gassmoeller, R., & Dannberg, J. (2021). *Mantle convection and possible mantle plumes beneath Antarctica – insights from geodynamic models and implications for topography* (Vol. 56). Geological Society. https://doi.org/10.1144/M56-2020-2

Brough, S., Carr, J. R., Ross, N., & Lea, J. M. (2019). Exceptional retreat of Kangerlussuaq glacier, East Greenland, between 2016 and 2018. *Frontiers in Earth Science*, *7*(123). https://doi.org/10.3389/feart.2019.00123

Cathles, L. M. (1975). *The viscosity of the earth's mantle*. (p. 386). Princeton University Press.

Celli, N. L., Lebedev, S., Schaeffer, A. J., & Gaina, C. (2021). The tilted Iceland plume and its effect on the North Atlantic evolution and magmatism. *Earth and Planetary Science Letters*, *569*, 117048. https://doi.org/10.1016/j.epsl.2021.117048

Crameri, F. (2018). Scientific colour maps. *Zenodo*. https://doi.org/10.5281/zenodo.1243862

Dziewonski, A. M., & Anderson, D. L. (1981). Preliminary reference Earth model. *Physics of the Earth and Planetary Interiors*, *25*(4), 297–356. https://doi.org/10.1016/0031-9201(81)90046-7

Gomez, N., Latychev, K., & Pollard, D. (2018). A coupled ice sheet–sea level model incorporating 3D Earth structure: Variations in Antarctica during the last deglacial retreat. *Journal of Climate*, *31*(10), 4041–4054. https://doi.org/10.1175/JCLI-D-17-0352.1

Gomez, N., Pollard, D., & Holland, D. (2015). Sea-level feedback lowers projections of future Antarctic Ice-Sheet mass loss. *Nature Communications*, *6*(8798). https://doi.org/10.1038/ncomms9798

Hansen, K., Truffer, M., Aschwanden, A., Mankoff, K., Bevis, M., Humbert, A., et al. (2021). Estimating ice discharge at Greenland's three largest outlet glaciers using local bedrock uplift. *Geophysical Research Letters*, *48*(14). https://doi.org/10.1029/2021GL094252

Hartmann, R., Ebbing, J., & Conrad, C. P. (2020). A Multiple 1D Earth Approach (M1DEA) to account for lateral viscosity variations in solutions of the sea level equation: An application for glacial isostatic adjustment by Antarctic deglaciation. *Journal of Geodynamics*, *135*, 101695. https://doi.org/10.1016/j.jog.2020.101695

Heeszel, D. S., Wiens, D. A., Anandakrishnan, S., Aster, R. C., Dalziel, I. W. D., Huerta, A. D., et al. (2016). Upper mantle structure of Central and West Antarctica from array analysis of Rayleigh wave phase velocities. *Journal of Geophysical Research: Solid Earth*, *121*(3), 1758–1775. https://doi.org/10.1002/2015JB012616

Helm, V., Humbert, A., & Miller, H. (2014). Elevation and elevation change of Greenland and Antarctica derived from CryoSat-2. *The Cryosphere*, *8*(4), 1539–1559. https://doi.org/10.5194/tc-8-1539-2014

Ivins, E. R., & Sammis, C. G. (1995). On lateral viscosity contrast in the mantle and the rheology of low-frequency geodynamics. *Geophysical Journal International*, *123*(2), 305–322. https://doi.org/10.1111/j.1365-246X.1995.tb06856.x

Ivins, E. R., van der Wal, W., Wiens, D. A., Lloyd, A. J., & Caron, L. (2021). *Antarctic upper mantle rheology* (Vol. 56). Geological Society. https://doi.org/10.1144/M56-2020-19

Kachuck, S. B., Martin, D. F., Bassis, J. N., & Price, S. F. (2020). Rapid viscoelastic deformation slows marine ice sheet instability at Pine Island Glacier. *Geophysical Research Letters*, *47*(10), e2019GL086446. https://doi.org/10.1029/2019GL086446

Kang, K., Zhong, S., Geruo, A., & Mao, W. (2022). The effects of non-Newtonian rheology in the upper mantle on relative sea level change and geodetic observables induced by glacial isostatic adjustment process. *Geophysical Journal International*, *228*(3), 1975–1991. https://doi.org/10.1093/gji/ggab428

Khan, S. A., Bjørk, A. A., Bamber, J. L., Morlighem, M., Bevis, M., Kjær, K. H., et al. (2020). Centennial response of Greenland's three largest outlet glaciers. *Nature Communications*, *11*(1), 5718. https://doi.org/10.1038/s41467-020-19580-5

Khan, S. A., Sasgen, I., Bevis, M., van Dam, T., Bamber, J. L., Wahr, J., et al. (2016). Geodetic measurements reveal similarities between post–Last glacial maximum and present-day mass loss from the Greenland Ice Sheet. *Science Advances*, *2*(9). https://doi.org/10.1126/sciadv.1600931

Konrad, H., Sasgen, I., Pollard, D., & Klemann, V. (2015). Potential of the solid-Earth response for limiting long-term West Antarctic Ice Sheet retreat in a warming climate. *Earth and Planetary Science Letters*, *432*, 254–264. https://doi.org/10.1016/j.epsl.2015.10.008

Lau, H. C. P., Austermann, J., Holtzman, B. K., Havlin, C., Lloyd, A. J., Book, C., & Hopper, E. (2021). Frequency dependent mantle viscoelasticity via the complex viscosity: Cases from Antarctica. *Journal of Geophysical Research: Solid Earth*, *126*(e2021JB022622). https://doi.org/10.1029/2021JB022622

Levermann, A., Clark, P. U., Marzeion, B., Milne, G. A., Pollard, D., Radic, V., & Robinson, A. (2013). The multimillennial sea-level commitment of global warming. *Proceedings of the National Academy of Sciences*, *110*(34), 13745–13750. https://doi.org/10.1073/pnas.1219414110

Lloyd, A. J., Wiens, D. A., Zhu, H., Tromp, J., Nyblade, A. A., Aster, R. C., et al. (2020). Seismic structure of the Antarctic upper mantle imaged with adjoint tomography. *Journal of Geophysical Research: Solid Earth*, *125*(3). https://doi.org/10.1029/2019JB017823

Marsman, C. P., van der Wal, W., Riva, R. E. M., & Freymueller, J. T. (2021). The impact of a 3-D Earth structure on glacial isostatic adjustment in southeast Alaska following the little ice age. *Journal of Geophysical Research: Solid Earth*, *126*(12), e2021JB022312. https://doi.org/10.1029/2021JB022312

Martos, Y. M., Jordan, T. A., Catalán, M., Jordan, T. M., Bamber, J. L., & Vaughan, D. G. (2018). Geothermal heat flux reveals the Iceland hotspot track underneath Greenland. *Geophysical Research Letters*, *45*(16), 8214–8222. https://doi.org/10.1029/2018GL078289

Milne, G. A., Latychev, K., Schaeffer, A., Crowley, J. W., Lecavalier, B. S., & Audette, A. (2018). The influence of lateral Earth structure on glacial isostatic adjustment in Greenland. *Geophysical Journal International*, *214*(2), 1252–1266. https://doi.org/10.1093/gji/ggy189

Mordret, A. (2018). Uncovering the Iceland hot spot track beneath Greenland. *Journal of Geophysical Research: Solid Earth*, *123*(6), 4922–4941. https://doi.org/10.1029/2017JB015104

Moresi, L., Dufour, F., & Mühlhaus, H.-B. (2003). A Lagrangian integration point finite element method for large deformation modeling of viscoelastic geomaterials. *Journal of Computational Physics*, *184*(2), 476–497. https://doi.org/10.1016/S0021-9991(02)00031-1

Nield, G. A., Barletta, V. R., Bordoni, A., King, M. A., Whitehouse, P. L., Clarke, P. J., et al. (2014). Rapid bedrock uplift in the Antarctic Peninsula explained by viscoelastic response to recent ice unloading. *Earth and Planetary Science Letters*, *397*, 32–41. https://doi.org/10.1016/j.epsl.2014.04.019

Pollard, D., Gomez, N., & Deconto, R. M. (2017). Variations of the Antarctic Ice Sheet in a coupled Ice Sheet-Earth-Sea Level Model: Sensitivity to viscoelastic Earth properties. *Journal of Geophysical Research: Earth Surface*, *122*(11), 2124–2138. https://doi.org/10.1002/2017JF004371

Ramirez, F., Selway, K., Conrad, C. P., & Lithgow-Bertelloni, C. (2022). Constraining upper mantle viscosity using temperature and water content inferred from seismic and magnetotelluric data. *Journal of Geophysical Research: Solid Earth*, *127*(8), e2021JB023824. https://doi.org/10.1029/2021JB023824

Rogozhina, I., Petrunin, A. G., Vaughan, A. P. M., Steinberger, B., Johnson, J. V., Kaban, M. K., et al. (2016). Melting at the base of the Greenland ice sheet explained by Iceland hotspot history. *Nature Geoscience*, *9*(5), 366–369. https://doi.org/10.1038/ngeo2689

Rose, I., Buffett, B., & Heister, T. (2017). Stability and accuracy of free surface time integration in viscous flows. *Physics of the Earth and Planetary Interiors*, *262*, 90–100. https://doi.org/10.1016/j.pepi.2016.11.007

Sandiford, D., Brune, S., Glerum, A., Naliboff, J. B., & Whittaker, J. M. (2021). Kinematics of footwall exhumation at oceanic detachment faults: Solid-block rotation and apparent unbending. *Geochemistry, Geophysics, Geosystems*, *22*(4), e2021GC009681. https://doi.org/10.1029/2021GC009681

Simpson, M. J. R., Wake, L., Milne, G. A., & Huybrechts, P. (2011). The influence of decadal-to millennial-scale ice mass changes on present-day vertical land motion in Greenland: Implications for the interpretation of GPS observations. *Journal of Geophysical Research*, *116*(B2), B02406. https://doi.org/10.1029/2010jb007776

Steffen, R., Audet, P., & Lund, B. (2018). Weakened lithosphere beneath Greenland inferred from effective elastic thickness: A hot spot effect? *Geophysical Research Letters*, *45*(10), 4733–4742. https://doi.org/10.1029/2017GL076885

Steinberger, B., Bredow, E., Lebedev, S., Schaeffer, A., & Torsvik, T. H. (2019). Widespread volcanism in the Greenland–North Atlantic region explained by the Iceland plume. *Nature Geoscience*, *12*(1), 61–68. https://doi.org/10.1038/s41561-018-0251-0

The IMBIE Team. (2018). Mass balance of the Antarctic Ice Sheet from 1992 to 2017. *Nature*, *558*(7709), 219–222. https://doi.org/10.1038/s41586-018-0179-y

The IMBIE Team. (2019). Mass balance of the Greenland Ice Sheet from 1992 to 2018. *Nature*, *579*(7798), 233–239. https://doi.org/10.1038/s41586-019-1855-2

van der Wal, W., Barnhoorn, A., Stocchi, P., Gradmann, S., Wu, P., Drury, M., & Vermeersen, L. L. A. (2013). Glacial isostatic adjustment model with composite 3-D Earth rheology for Fennoscandia. *Geophysical Journal International*, *194*(1), 61–77. https://doi.org/10.1093/gji/ggt099

van der Wal, W., Whitehouse, P. L., & Schrama, E. J. O. (2015). Effect of GIA models with 3D composite mantle viscosity on GRACE mass balance estimates for Antarctica. *Earth and Planetary Science Letters*, *414*, 134–143. https://doi.org/10.1016/j.epsl.2015.01.001

Whitehouse, P. L. (2018). Glacial isostatic adjustment modelling: Historical perspectives, recent advances, and future directions. *Earth Surface Dynamics*, *6*(2), 401–429. https://doi.org/10.5194/esurf-6-401-2018

Whitehouse, P. L., Gomez, N., King, M. A., & Wiens, D. A. (2019). Solid Earth change and the evolution of the Antarctic Ice Sheet. *Nature Communications*, *10*(503). https://doi.org/10.1038/s41467-018-08068-y

Wolstencroft, M., King, M. A., Whitehouse, P. L., Bentley, M. J., Nield, G. A., King, E. C., et al. (2015). Uplift rates from a new high-density GPS network in Palmer land indicate significant late Holocene ice loss in the southwestern Weddell Sea. *Geophysical Journal International*, *203*(1), 737–754. https://doi.org/10.1093/gji/ggv327

Zeitz, M., Haacker, J. M., Donges, J. F., Albrecht, T., & Winkelmann, R. (2022). Dynamic regimes of the Greenland Ice Sheet emerging from interacting melt-elevation, and glacial isostatic adjustment feedbacks. *Earth System Dynamics*, *13*(3), 1077–1096. https://doi.org/10.5194/esd-13-1077-2022